ADVANCED FUNCTIONAL MATERIALS
www.afm-journal.de

Wide Field Magnetic Luminescence Imaging

*Matthew P. P. Hodges, Martin Grell, Nicola A. Morley, and Dan A. Allwood**

This study demonstrates how magnetic-field-dependent luminescence from organic films can be used to image the magnetic configuration of an underlying sample. The organic semiconductors tetracene and rubrene exhibit singlet exciton fission, which is a process sensitive to magnetic fields. Here, thin films of these materials were characterized using photoluminescence spectrometry, atomic force microscopy, and photoluminescence magnetometry. The luminescence from these substrate-bound thin films is imaged to reveal the magnetic configuration of underlying Nd-Fe-B magnets. The tendency of rubrene to form amorphous films and produce large changes in photoluminescence under an applied magnetic field makes it more appropriate for magnetic field imaging than tetracene. This demonstration can be extended in the future to allow simple microscopic imaging of magnetic structure.

1. Introduction

Magnetic microscopy is invaluable for studying magnetic domain configurations and dynamics in bulk, thin film, and patterned samples.[1–6] The ideal form of magnetic microscopy will offer high spatial resolution, high temporal resolution, and high sensitivity to magnetization, magnetic moment, or magnetic field. It is also desirable that the technique should be nondestructive, nonperturbing, rapid, and affordable. Numerous magnetic microscopy techniques now exist that can readily deliver on many of these criteria, however no single approach can satisfy them all, and must therefore be used in a complementary manner. For example, Lorentz microscopy offers extremely high spatial resolution (sub-5 nm) but requires electron-transparent samples and temporal resolution remains challenging.[7] Beamline techniques such as magnetic transmission X-ray microscopy (M-TXM)[8,9] and X-ray magnetic circular dichroism photoelectron emission microscopy (XMCD-PEEM)[10,11] combine high spatial resolution (sub-10 nm[12,13] for M-TXM, sub-50 nm for XMCD-PEEM[14,15]) with ultrafast temporal resolution,[16] but require a synchrotron light source to operate and either the sample to be operated in a vacuum (XMCD-PEEM) or be X-ray transparent (M-TXM).[17,18] Magneto-optical microscopy can offer ultrafast (sub-ps) temporal resolution, but has moderate spatial resolution,[19] unless delicate near-field approaches are used.[20] Scanning probe techniques such as magnetic force microscopy (MFM) and scanning Hall probe microscopy (SHPM) offer a versatile laboratory-scale platform with high spatial resolution (sub-10 nm for MFM,[21] sub-200 nm for SHPM[22]), but have poor temporal resolution.[1] Recently, a single spin scanning probe magnetometry technique has been developed[23–27] that uses an optically detected magnetic resonance from a nitrogen vacancy-doped diamond probe to resolve magnetic fields above samples achieving high spatial resolution (sub-20 nm) and high sensitivity (sub-10 μT $Hz^{-1/2}$), but requires time averaging that limits temporal resolution.

Here, we describe the development of a wide-field optical imaging technique of magnetic fields based upon the "magnetic field effect" of photoluminescence.[28–33] This refers to the magnetic field-dependent photoluminescence exhibited most commonly by some organic semiconductors and certain organometallic complexes. The strength of this magnetic photoluminescence (MPL) is usually described as

$$\mathrm{MPL} = \frac{I_\mathrm{H} - I_0}{I_0} \times 100\% \quad (1)$$

where I_H and I_0 are the photoluminescent intensities observed with and without an applied magnetic field, respectively. It has been observed to exceed 20% in some materials and tends to display a nonlinear response with magnetic field.[34,35] MPL is described by singlet exciton fission.[36] This phenomenon arises due to the coupling of a molecule in the electronic singlet ground state S_0 with a nearby molecule in the first excited singlet state S_1 to form a "correlated triplet-pair state" ^{1}(TT), at a rate proportional to the rate constant k_{-2}, which can then go on to dissociate into separate triplet states T_1, described by

$$S_1 + S_0 \underset{k_2}{\overset{k_{-2}}{\rightleftharpoons}} {}^1(\mathrm{TT}) \underset{k_1}{\overset{k_{-1}}{\rightleftharpoons}} T_1 + T_1 \quad (2)$$

The singlet character of the ^{1}(TT) state determines the probability of dissociating into the two discrete triplet excitons ($T_1 + T_1$), proportional to the rate constant k_{-1}, shown in Equation (2), rather than two discrete singlet states ($S_1 + S_0$),

Dr. M. P. P. Hodges, Dr. N. A. Morley, Prof. D. A. Allwood
Department of Materials Science and Engineering
University of Sheffield
Sheffield S1 3JD, UK
E-mail: d.allwood@sheffield.ac.uk
Dr. M. Grell
Department of Physics and Astronomy
University of Sheffield
Sheffield S3 7RH, UK

DOI: 10.1002/adfm.201606613

proportional to the rate constant k_2, respectively. In the case of an MPL sample with randomly oriented molecules, three of the nine possible ^{1}(TT) states possess singlet character when no external magnetic field is present. In the "low" magnetic field regime (typically <100 mT) the number of states possessing singlet character increases due to an interplay between Zeeman splitting, imposed by the applied magnetic field, and spin–spin interactions until all nine states have singlet character, but reduces to just two states with singlet character in the "high" magnetic field regime (typically >100 mT). Therefore, a magnetic field applied to a singlet exciton fission material is able to affect the steady-state singlet/triplet exciton populations by varying the number of triplet pair states that have singlet character. This variation is represented by a change in the singlet fission rate, which in turn, results in a modification of the observed prompt and delayed fluorescence.[32,35]

Here we show that magnetic photoluminescence offers a convenient method of measuring magnetic fields that are present in the local sample environment. By imaging the photoluminescence of an organic thin film of material exhibiting MPL we show that it is possible to visualize the magnetic stray field of permanent magnets lying close behind the film substrate.

2. Results and Discussion

Absorption and photoluminescence spectrophotometry of tetracene (**Figure 1**a) showed a smaller Stokes shift than for rubrene (Figure 1b). These spectra agree very closely with previous measurements of polycrystalline tetracene[37] and amorphous rubrene.[32] Atomic force microscopy measurements of tetracene samples confirmed a granular structure (**Figure 2**a), most likely due to island growth, which has been predicted theoretically[38] and seen experimentally.[39] The grain size obtained (≈0.25–0.50 µm in diameter) depends on a number of factors including deposition rate, substrate material, substrate temperature during growth, and film thickness.[40] Similar measurements of rubrene films (Figure 2b) revealed an amorphous (or highly polycrystalline) morphology with a surface roughness <5 nm. This is in contrast to another thin film of rubrene, shown in Figure 2c, which showed spherulite formation, possibly due to nucleation of the polycrystalline phase.[41]

MPL measurements of polycrystalline tetracene, amorphous rubrene, and polycrystalline rubrene films are shown in

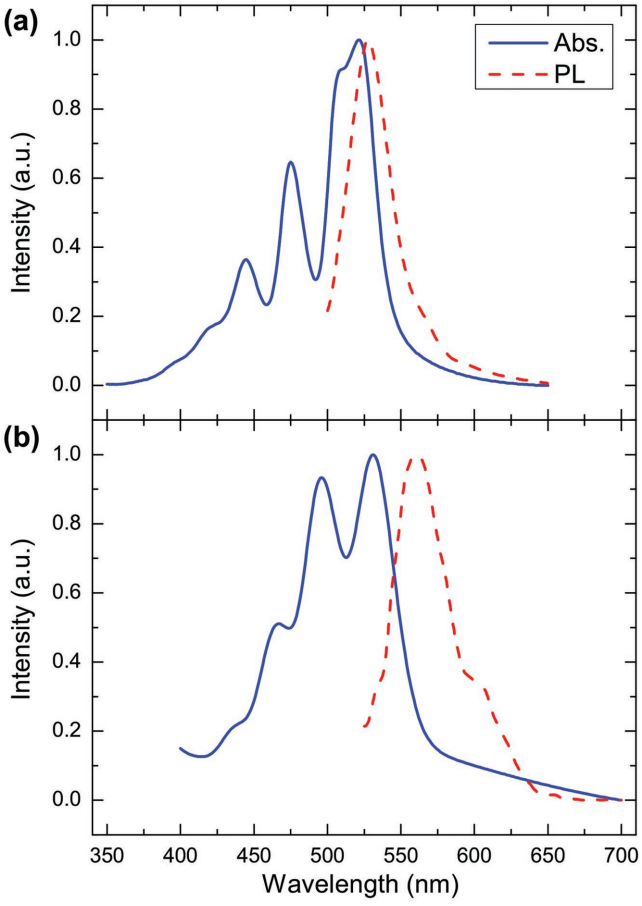

Figure 1. Normalized absorption spectra (solid blue lines) and photoluminescence spectra (dashed red lines) from a) polycrystalline tetracene and b) amorphous rubrene thin films measured at room temperature.

Figure 3. For polycrystalline tetracene the MPL initially reduces to −3.1% at 20 mT before returning to the zero magnetic field intensity at 50 mT. Above 50 mT the MPL becomes positive reaching +9.8% at 295 mT. For amorphous rubrene the relative change in photoluminescent intensity initially reduces to −3.5% at 25 mT before returning to the zero magnetic field intensity at 70 mT. Above 70 mT the relative change in intensity becomes positive reaching +24.4% at 295 mT. Rubrene, when illuminated by light and exposed to oxygen, undergoes

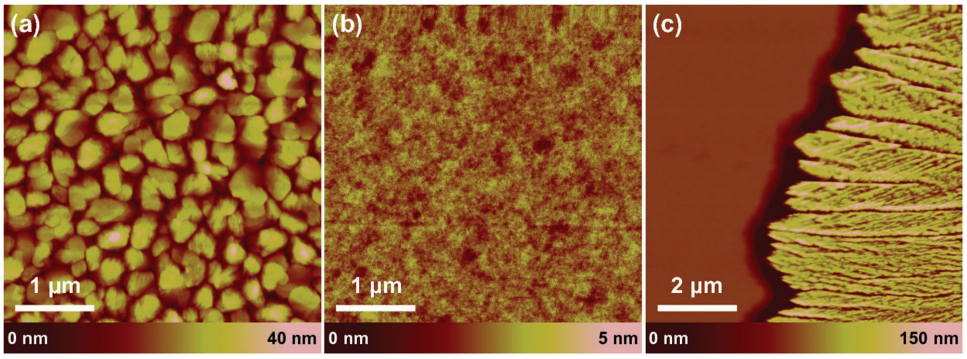

Figure 2. Atomic force microscopy images of a thin film of a) polycrystalline tetracene, b) amorphous rubrene, and c) polycrystalline rubrene.

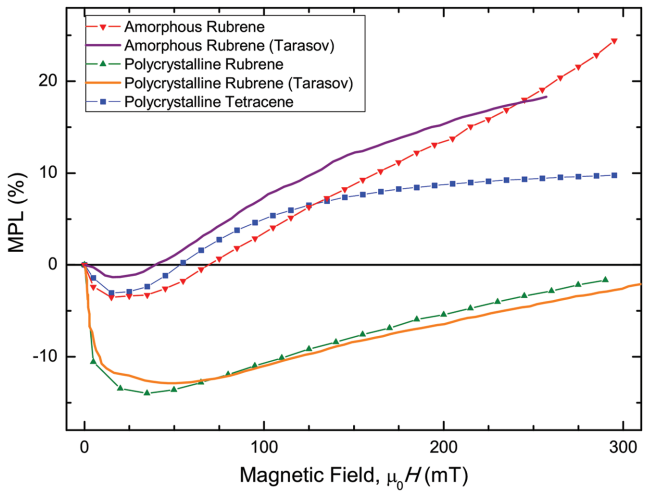

Figure 3. Plot of magnetic photoluminescence as a function of magnetic field for tetracene and rubrene. Tarasov et al. plots have been included for comparison.[48] All measurements were performed under standard ambient temperature and pressure conditions.

photo-oxidation, chemically altering the rubrene causing irreversible photobleaching.[42] Therefore, to achieve the largest MPL before significant photo-oxidation occurred, the amorphous rubrene MPL measurement was performed in reverse order from high to low magnetic field. A reverse measurement was also performed for polycrystalline tetracene but no significant difference in the profile was observed suggesting that photo-oxidation in tetracene is negligible over the timescale of the measurement. The amorphous rubrene MPL measurements in Figure 3 agree with those of Tarasov et al.[48] performed in a vacuum. The similarity of these results is despite Tarasov et al. using much thicker films than those used here and confirms the independence of singlet fission dynamics upon film thickness.[43]

The MPL measurement for polycrystalline rubrene also showed a large decrease in photoluminescence (−11.6%) at low magnetic field followed by a monotonic increase approaching 0% MPL at high magnetic field (Figure 3), again, in good agreement with similar measurements by Tarasov et al.[48]

In preparation for MPL imaging, Hall sensor imaging of the magnetic field above the permanent magnets was undertaken (**Figure 4**), which, for the pair of cubic magnets with their poles oriented in-plane (Figure 4b,d), showed a bipolar field profile with a measured peak field of ±247 mT. The ring-shaped magnet, with its poles oriented out-of-plane, showed an asymmetrical field intensity with a peak field of +299 mT. Example raw input images and magnetic contrast difference images (with and without the underlying Nd-Fe-B magnets) from tetracene and amorphous rubrene films are shown in **Figure 5**a–c and Figure 5d–f, respectively. The tetracene contrast image generated by the magnetic stray field of the ring-shaped magnet shows a clearly defined region of circular contrast with light and dark concentric bands. For the contrast images featuring cubic magnets, both tetracene (Figure 5e) and rubrene (Figure 5f) produced two lobes of strong, nonuniform MPL contrast in response to magnetic stray field from the magnets. The unipolar nature of the features here indicates that the MPL imaging is sensitive to field magnitude only but nonetheless reflect the general form of the Hall sensor measurement (Figure 4b,d) very closely. However, the MPL characteristic for tetracene and rubrene (Figure 3) can be used to explore the quantitative aspects of MPL imaging. In the tetracene magnetic contrast image (Figure 5e,h), the darkest regions have a minimum MPL of −3.1%, which corresponds to $\mu_0 H$ = 20 mT (Figure 3). The brightest regions show a maximum MPL of 9.3%, which correspond to $\mu_0 H$ = 247 mT, which was the peak field as measured by the Hall array sensor (Figure 4d). Identical behavior was observed with the amorphous rubrene images (Figure 5f,i) with minimum and maximum MPL values of −3.5% and 18% again corresponding to $\mu_0 H$ = 25 mT and

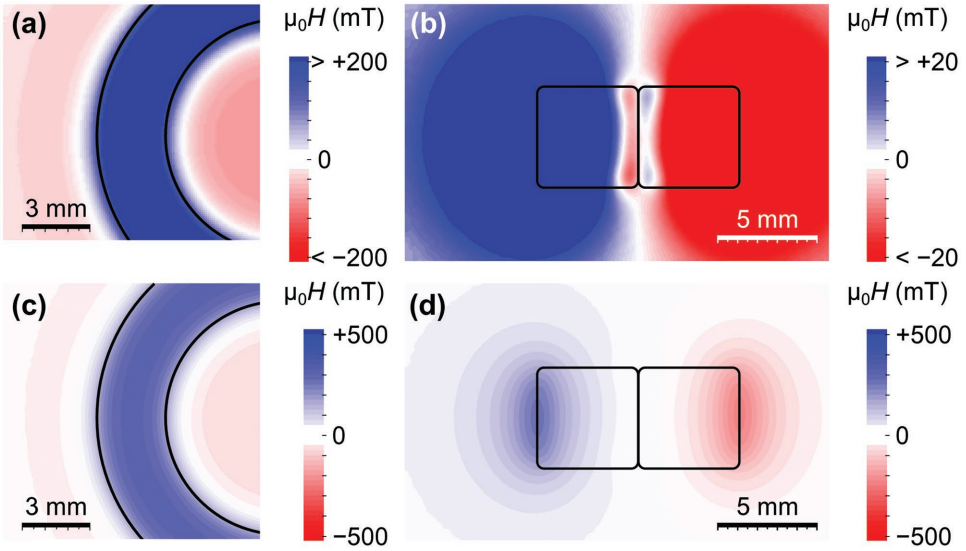

Figure 4. Magnetic stray field maps of a,c) a portion of the ring-shaped Nd-Fe-B permanent magnet and b,d) two cubic Nd-Fe-B permanent magnets, both measured experimentally by a commercial 2D Hall sensor array device scaled to the range a) ±200 mT, b) ±20 mT, and c,d) ±500 mT. The peak magnetic field, $\mu_0 H_{max}$ = +299 mT for the ring-shaped permanent magnet and $\mu_0 H_{max}$ = ±247 mT for the two cubic permanent magnets.

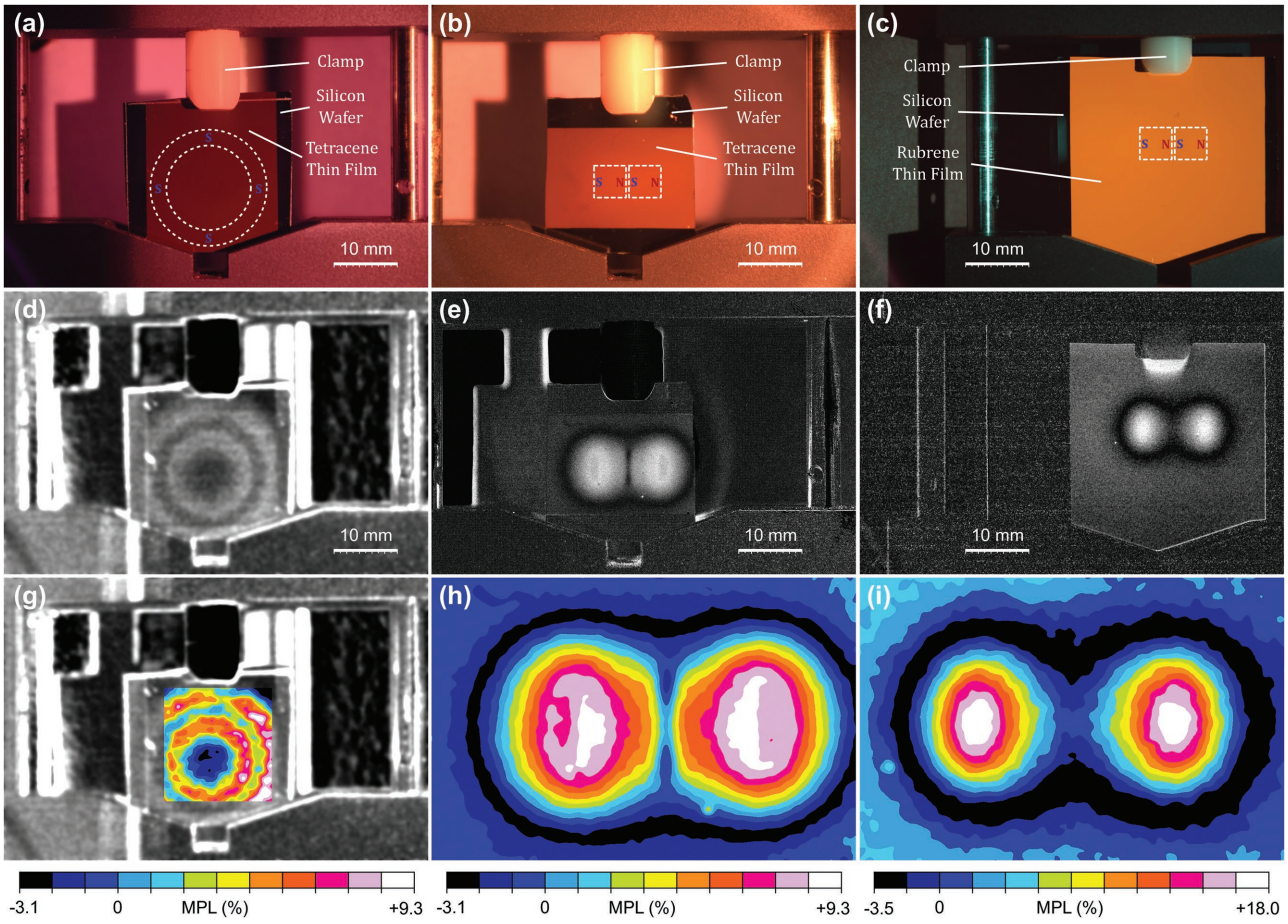

Figure 5. a–c) The first row contains photographs d–f) used to calculate difference images of MPL contrast presented in the second row. The dashed lines represent the position of the permanent magnets behind the silicon substrates. False color images of the MPL contrast is shown in the third row g–i) approximately quantifying the MPL magnitude. a,d,g) The first column demonstrates a ring-shaped permanent magnet's stray field generating MPL contrast in a polycrystalline tetracene thin film. b,e,h) The second and c,f,i) third column demonstrate the same phenomenon for a pair of cubic permanent magnets positioned behind thin films of polycrystalline tetracene and amorphous rubrene, respectively.

247 mT from the amorphous rubrene MPL characteristic (Figure 3). The standard error for the ring-shaped magnet tetracene contrast image (Figure 5d), the cubic magnet tetracene contrast image (Figure 5e), and the cubic magnet amorphous rubrene contrast image (Figure 5f) was measured to be 0.048, 0.053, and 0.093, respectively. The maximum spatial resolution of the current experimental arrangement is estimated to be 19 µm based on the camera's pixel resolution (3504 × 2336). The temporal resolution of this arrangement is on the order of minutes due to each image requiring ≈5 min exposure time. This time could be significantly reduced with a high-efficiency, low-noise monochrome camera, and thermoelectrically cooled charge-coupled device (CCD) cameras are likely to be capable of detecting the MPL contrast without the need to perform difference imaging.

Although the MPL images here (Figure 5) are of a macroscopic system, they open the possibility of microscopic imaging using MPL from films on magnetic surfaces. Sample preparation would be straightforward and films such as tetracene and rubrene are removed readily with appropriate solvents to return the sample to its original state after imaging. The unique characteristics of MPL imaging may allow several new opportunities in imaging field from magnetization configurations. MPL imaging could be performed with either wide-field or scanning systems and with continuous or pulsed excitation sources, although temporal resolution would, in the case of room temperature amorphous rubrene, be limited by the 2.2 ns relaxation rate of the photoluminescent film.[32] The optical working distances and nonreflective nature of MPL imaging may even allow magnetization structure of rough surfaces or the surface of 3D objects[44] to be resolved. The fields from magnetic features such as domain walls in soft magnetic nanowires are of an appropriate magnitude for MPL detection[45,46] and imaging could be extended to microscopic length-scales. The luminescent nature of singlet exciton fission-based magnetic microscopy means that it may be possible to employ stimulated emission-depletion microscopy approaches to achieve subdiffraction limit resolution.[47] This would require further effort to determine the appropriate wavelengths to promote stimulated emission in the luminescent layers.

MPL imaging must overcome two challenges in particular to progress. First, the bipolar MPL response of polycrystalline tetracene and amorphous rubrene to an applied magnetic field (Figure 3) introduces ambiguity in determining the field

magnitude. A simple way of resolving this would be to use materials with a unipolar MPL response, such as polycrystalline rubrene, however, spatial resolution of any MPL-based microscopy technique would be limited by the grain size of the organic film. Instead, it may be possible to overcome the bipolar MPL response by increasing the thickness of the organic layer. This would select the weaker magnetic fields that exist further from the underlying magnetic sample and could match the maximum detected magnetic field to that for achieving minimum MPL, albeit at the expense of spatial resolution. Alternatively, a small, uniform bias field could be applied to successive images to remove the ambiguity. The second issue is the response and stability of the luminescent materials used so far to achieve MPL imaging. Tetracene offers good stability in standard laboratory conditions, but has an MPL less than half that of rubrene (Figure 3). Furthermore, the polycrystalline nature of thermally evaporated tetracene thin films could limit spatial resolution in microscopy. Rubrene, meanwhile, has over twice the MPL of tetracene and can be deposited as an amorphous thin film, but has poor stability in standard laboratory conditions due to rapid photobleaching caused by photo-oxidation. This limitation may be overcome by depositing an optically transparent barrier layer on top of the rubrene thin film or to store and perform imaging of rubrene in a suitable solvent or inert atmosphere.

3. Conclusions

Magnetic imaging of macroscopic permanent magnets via exploitation of the singlet exciton fission phenomenon has been demonstrated using two different photoluminescent organic semiconductors. This proof of concept demonstrates that there are no intrinsic barriers preventing this technique from operating at microscopic length-scales; i.e., the ability to perform microscopic imaging of magnetic structures. Furthermore, two promising candidate materials (polycrystalline tetracene and amorphous rubrene) have been identified for the technique that can generate large changes in photoluminescence (9.8% and 24.4%, respectively) in response to an applied magnetic field.

4. Experimental Section

Tetracene and rubrene powders (Sigma-Aldrich; sublimed grade at 99.99% purity) were selected as they have been shown to produce large MPL at room temperature.[30,35,48,49] These were thermally evaporated (base pressure $\approx 5 \times 10^{-5}$ Pa) onto Si (001) and quartz substrates (lateral dimensions $\approx 40 \times 40$ mm^2) at a rate of 1.5 nm s^{-1}. Film thicknesses were measured by atomic force microscopy (Bruker Dimension 3100 Atomic Force Microscope) to be 80 ± 1 nm. Samples were wrapped in aluminum foil and stored under vacuum to minimize any deterioration before use.

Absorption spectrophotometry of the thin films evaporated onto quartz substrates was performed using a Perkin–Elmer Lambda 900 spectrometer while photoluminescence spectrophotometry of the thin films evaporated onto silicon substrates was performed using a Perkin–Elmer LS-50B photoluminescence spectrometer.

The MPL response of each sample was characterized using a custom-built photoluminescence magnetometry system (**Figure 6**a). The samples were placed between the pole pieces of an electromagnet and excited with continuous-wave visible light of wavelength 500 nm from a 1 W light emitting diode (LED). The electromagnet was turned on and off repeatedly for each magnetic field, $\mu_0 H$, from 0 mT up to 275–295 mT in 10–30 mT steps. An avalanche photodiode (APD) module (Hamamatsu C5460) fitted with an appropriate long-pass dichroic filter (transition wavelength = 650 nm for tetracene and 550 nm for rubrene) was used to capture the MPL, while an analog-to-digital converter (National Instruments USB-6212) sampled the APD signal at a rate of 262 144 samples per second. All experimental data were stored to a computer file for analysis.

Magnetic contrast images were obtained using a custom-built imaging system (Figure 6b). An MPL sample was placed directly in front of one of two magnetic sources: a pair of cubic $Nd_2Fe_{14}B$ permanent magnets (each measuring $5 \times 5 \times 5$ mm) and a ring-shaped $Nd_2Fe_{14}B$ permanent magnet (O.D. = 18 mm; I.D. = 13 mm; thickness = 3 mm). The sample was then excited, exactly as described above, in a lightproof enclosure. A Canon 50D digital SLR camera, fitted with an appropriate long-pass filter (identical to the previously described measurement

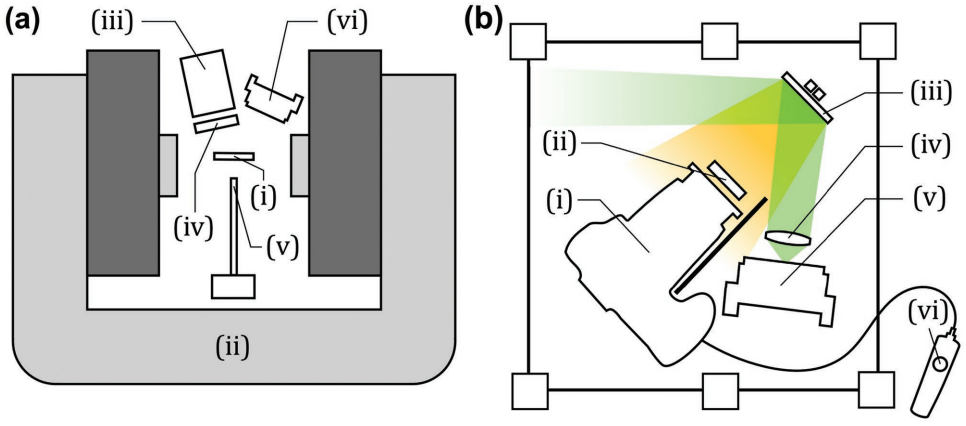

Figure 6. a) Schematic diagram of the custom-built MPL measurement system. The system, which was optically isolated in a lightproof enclosure, comprised of (i) the sample, which was placed between the pole pieces of (ii) the electromagnet, (iii) an avalanche photodiode (APD) for detection of photoluminescence, (iv) a long pass filter (LPF) to prevent non-photoluminescent light reaching the APD, (v) a Hall probe for measuring the magnetic field produced by the electromagnet, and (vi) a light-emitting diode (LED) light source for excitation of the photoluminescent sample. b) Schematic diagram of the MPL imaging system, which was also optically isolated in a lightproof enclosure. It comprised of a (i) Canon 50D digital camera for capturing images of the whole sample, (ii) a long-pass filter for preventing non-photoluminescent light reaching the camera, (iii) the sample and two Nd-Fe-B permanent magnets, (iv) a focusing lens, (v) an LED light source for exciting the photoluminescent sample, and (vi) a shutter release remote control that allowed for remote operation of the camera.

system), was used to image the MPL generated by the sample. For each MPL image, two photographs were taken with and without the Nd-Fe-B magnets directly behind the center of each sample. The difference of these two photographs was then calculated using the image analysis software ImageJ.[50] For comparison, the magnetic field of the Nd-Fe-B magnets were measured using a commercial Hall sensor array camera.[51]

Acknowledgements

The authors thank EPSRC for a DTA Ph.D. studentship and the University of Sheffield for MH's Postdoctoral Fellowship in support of this work.

Conflict of Interest

The authors declare no conflict of interest.

Keywords

magnetic imaging, photoluminescence, rubrene, singlet exciton fission, tetracene

Received: December 14, 2016
Revised: March 3, 2017
Published online:

[1] M. R. Freeman, B. C. Choi, *Science* **2001**, *294*, 1484.
[2] H. Hopster, H. P. Oepen, *Magnetic Microscopy of Nanostructures*, Springer-Verlag, Berlin **2005**.
[3] I. Manke, N. Kardjilov, R. Schäfer, A. Hilger, M. Strobl, M. Dawson, C. Grünzweig, G. Behr, M. Hentschel, C. David, A. Kupsch, A. Lange, J. Banhart, *Nat. Commun.* **2010**, *1*, 125.
[4] O. Boulle, J. Vogel, H. Yang, S. Pizzini, D. de Souza Chaves, A. Locatelli, T. O. Menteş, A. Sala, L. D. Buda-Prejbeanu, O. Klein, M. Belmeguenai, Y. Roussigné, A. Stashkevich, S. M. Chérif, L. Aballe, M. Foerster, M. Chshiev, S. Auffret, I. M. Miron, G. Gaudin, *Nat. Nanotechnol.* **2016**, *11*, 449.
[5] C. Blanco-Roldan, C. Quiros, A. Sorrentino, A. Hierro-Rodriguez, L. M. Alvarez-Prado, R. Valcarcel, M. Duch, N. Torras, J. Esteve, J. I. Martin, M. Velez, J. M. Alameda, E. Pereiro, S. Ferrer, *Nat. Commun.* **2015**, *6*, 8196.
[6] S. H. Yang, K. S. Ryu, S. Parkin, *Nat. Nanotechnol.* **2015**, *10*, 221.
[7] S. Amelinckx, D. van Dyck, J. van Landuyt, G. van Tendeloo, *Handbook of Microscopy, Handbook of Microscopy: Applications in Materials Science, Solid-State Physics, and Chemistry. Methods II*, Wiley, Hoboken, NJ **2008**.
[8] V. Uhlir, M. Urbanek, L. Hladik, J. Spousta, M. Y. Im, P. Fischer, N. Eibagi, J. J. Kan, E. E. Fullerton, T. Sikola, *Nat. Nanotechnol.* **2013**, *8*, 341.
[9] W. Chao, B. D. Harteneck, J. A. Liddle, E. H. Anderson, D. T. Attwood, *Nature* **2005**, *435*, 1210.
[10] K. Y. Guslienko, X. F. Han, D. J. Keavney, R. Divan, S. D. Bader, *Phys. Rev. Lett.* **2006**, *96*, 4.
[11] H. Jung, Y. S. Yu, K. S. Lee, M. Y. Im, P. Fischer, L. Bocklage, A. Vogel, M. Bolte, G. Meier, S. K. Kim, *Appl. Phys. Lett.* **2010**, *97*, 3.
[12] C. Phatak, A. K. Petford-Long, M. De Graef, *Curr. Opin. Solid State Mater. Sci.* **2016**, *20*, 107.
[13] S. McVitie, D. McGrouther, S. McFadzean, D. A. MacLaren, K. J. O'Shea, M. J. Benitez, *Ultramicroscopy* **2015**, *152*, 57.
[14] J. Stöhr, A. Scholl, T. J. Regan, S. Anders, J. Lüning, M. R. Scheinfein, H. A. Padmore, R. L. White, *Phys. Rev. Lett.* **1999**, *83*, 1862.
[15] S. Da Col, S. Jamet, N. Rougemaille, A. Locatelli, T. O. Mentes, B. S. Burgos, R. Afid, M. Darques, L. Cagnon, J. C. Toussaint, O. Fruchart, *Phys. Rev. B* **2014**, *89*, 180405.
[16] D. Neeb, A. Krasyuk, A. Oelsner, S. A. Nepijko, H. J. Elmers, A. Kuksov, C. M. Schneider, G. Schonhense, *J. Phys.: Condens. Matter* **2005**, *17*, S1381.
[17] P. Fischer, G. Schutz, G. Schmahl, P. Guttmann, D. Raasch, *Z. Phys. B: Condens. Matter* **1996**, *101*, 313.
[18] P. Fischer, T. Eimuller, G. Schutz, G. Bayreuther, S. Tsunashima, N. Takagi, G. Denbeaux, D. Attwood, *J. Synchrotron Radiat.* **2001**, *8*, 325.
[19] J. Li, M. S. Lee, W. He, B. Redeker, A. Remhof, E. Amaladass, C. Hassel, T. Eimuller, *Rev. Sci. Instrum.* **2009**, *80*, 073703.
[20] B. L. Petersen, A. Bauer, G. Meyer, T. Crecelius, G. Kaindl, *Appl. Phys. Lett.* **1998**, *73*, 538.
[21] Y. Lisunova, J. Heidler, I. Levkivskyi, I. Gaponenko, A. Weber, C. Caillier, L. J. Heyderman, M. Klaui, P. Paruch, *Nanotechnology* **2013**, *24*, 8.
[22] J. S. Neal, H. G. Roberts, M. R. Connolly, S. Crampin, S. J. Bending, G. Wastlbauer, J. A. C. Bland, *Ultramicroscopy* **2006**, *106*, 614.
[23] L. Rondin, J.-P. Tetienne, P. Spinicelli, C. Dal Savio, K. Karrai, G. Dantelle, A. Thiaville, S. Rohart, J.-F. Roch, V. Jacques, *Appl. Phys. Lett.* **2012**, *100*, 153118.
[24] L. Rondin, J. P. Tetienne, S. Rohart, A. Thiaville, T. Hingant, P. Spinicelli, J. F. Roch, V. Jacques, *Nat. Commun.* **2013**, *4*, 2279.
[25] M. Pelliccione, A. Jenkins, P. Ovartchaiyapong, C. Reetz, E. Emmanouilidou, N. Ni, A. C. Bleszynski Jayich, *Nat. Nanotechnol.* **2016**, *11*, 700.
[26] D. Le Sage, K. Arai, D. R. Glenn, S. J. DeVience, L. M. Pham, L. Rahn-Lee, M. D. Lukin, A. Yacoby, A. Komeili, R. L. Walsworth, *Nature* **2013**, *496*, 486.
[27] J. P. Tetienne, T. Hingant, L. J. Martínez, S. Rohart, A. Thiaville, L. H. Diez, K. Garcia, J. P. Adam, J. V. Kim, J. F. Roch, I. M. Miron, G. Gaudin, L. Vila, B. Ocker, D. Ravelosona, V. Jacques, *Nat. Commun.* **2015**, *6*, 6733.
[28] R. E. Merrifield, *J. Chem. Phys.* **1968**, *48*, 4318.
[29] G. Klein, R. Voltz, M. Schott, *Chem. Phys. Lett.* **1972**, *16*, 340.
[30] J. Kalinowski, J. Godlewski, *Chem. Phys. Lett.* **1975**, *36*, 345.
[31] V. Ern, R. Merrifield, *Phys. Rev. Lett.* **1968**, *21*, 609.
[32] G. B. Piland, J. J. Burdett, D. Kurunthu, C. J. Bardeen, *J. Phys. Chem. C* **2013**, *117*, 1224.
[33] R. E. Merrifield, *Pure Appl. Chem.* **1971**, *27*, 481.
[34] C. Garditz, A. G. Muckl, M. Colle, *J. Appl. Phys.* **2005**, *98*, 093719.
[35] Y. Zhang, Y. Lei, Q. Zhang, Z. Xiong, *Org. Electron.* **2014**, *15*, 577.
[36] M. B. Smith, J. Michl, in *Annual Review of Physical Chemistry*, Vol. *64* (Eds: M. A. Johnson, T. J. Martinez), Annual Reviews, Palo Alto, CA **2013**, p. 361.
[37] S. T. Roberts, R. E. McAnally, J. N. Mastron, D. H. Webber, M. T. Whited, R. L. Brutchey, M. E. Thompson, S. E. Bradforth, *J. Am. Chem. Soc.* **2012**, *134*, 6388.
[38] S. Verlaak, S. Steudel, P. Heremans, D. Janssen, M. S. Deleuze, *Phys. Rev. B* **2003**, *68*, 195409.
[39] F. Cicoira, C. Santato, F. Dinelli, M. Murgia, M. A. Loi, F. Biscarini, R. Zamboni, P. Heremans, M. Muccini, *Adv. Funct. Mater.* **2005**, *15*, 375.
[40] A. Fahrenbruch and R. Bube, *Fundamentals of Solar Cells: Photovoltaic Solar Energy Conversion*, Elsevier Science, Amsterdam **2012**.
[41] C. E. Carraher, *Seymour/Carraher's Polymer Chemistry*, 6th ed., CRC Press, Boca Raton, FL **2003**.
[42] D. D. T. Mastrogiovanni, J. Mayer, A. S. Wan, A. Vishnyakov, A. V. Neimark, V. Podzorov, L. C. Feldman, E. Garfunkel, *Sci. Rep.* **2014**, *4*, 6.

[43] D. H. Arias, J. L. Ryerson, J. D. Cook, N. H. Damrauer, J. C. Johnson, *Chem. Sci.* **2016**, *7*, 1185.
[44] A. Fernández-Pacheco, L. Serrano-Ramón, J. M. Michalik, M. R. Ibarra, J. M. De Teresa, L. O'Brien, D. Petit, J. Lee, R. P. Cowburn, *Sci. Rep.* **2013**, *3*, 1492.
[45] D. A. Allwood, G. Xiong, C. C. Faulkner, D. Atkinson, D. Petit, R. P. Cowburn, *Science* **2005**, *309*, 1688.
[46] A. D. West, T. J. Hayward, K. J. Weatherill, T. Schrefl, D. A. Allwood, I. G. Hughes, *J.Phys. D: Appl. Phys.* **2012**, *45*, 095002.
[47] S. W. Hell, *Science* **2007**, *316*, 1153.
[48] V. V. Tarasov, G. E. Zoriniants, A. I. Shushin, M. M. Triebel, *Chem. Phys. Lett.* **1997**, *267*, 58.
[49] R. P. Groff, P. Avakian, R. E. Merrifield, *Phys. Rev. B* **1970**, *1*, 815.
[50] C. A. Schneider, W. S. Rasband, K. W. Eliceiri, *Nat. Methods* **2012**, *9*, 671.
[51] K. Vervaeke, *presented at 1st Int. Electric Drives Production Conf. (EDPC)*, Nuremberg, Germany, Sept **2011**.